H-Bond Stability in the tRNA^{Asp} Anticodon Hairpin: 3 ns of Multiple Molecular Dynamics Simulations

Pascal Auffinger and Eric Westhof
Institut de Biologie Moléculaire et Cellulaire du CNRS, Modélisations et Simulations des Acides Nucléiques, 67084 Strasbourg Cedex, France

ABSTRACT Multiple molecular dynamics trajectories of the solvated and neutralized 17-residue tRNA^{Asp} anticodon hairpin were generated for a total of 3 ns. Explicit treatment of all long-ranged electrostatic interactions by the particle mesh Ewald algorithm, as implemented in the AMBER MD software package, effected a degree of structural stabilization not previously achieved by use of a long 16-Å solvent interaction truncation scheme. The increased stability of this multiple molecular dynamics set was appropriate for an in-depth analysis of the six 500-ps-long trajectories and allowed the characterization of a number of key structural interactions. The dynamical behavior of the standard Watson–Crick base pairs, the noncanonical G30-U40 "wobble" base pair, and the Ψ32–C38 pseudo-base pair is presented as well as that of two C—H · · · O hydrogen bonds found to contribute to the array of tertiary interactions that stabilize the seven-nucleotide native loop conformation. The least mobile residue in the loop is U33, which forms the U-turn motif and which participates in several hydrogen-bonding interactions, whereas the most mobile residue is the apical residue G34 at the wobble position, a factor undoubtedly important in its biological function. The set of multiple molecular dynamics trajectories obtained does not converge on a 500-ps time scale to a unique dynamical model but instead describes an ensemble of structural microstates accessible to the system under the present simulation protocol, which is the result of local structural heterogeneity rather than of global conformational changes.

INTRODUCTION

The tertiary topology of known biological structures conveys the importance and diversity of hydrogen-bonding interactions in the maintenance of their native conformations (Jeffrey and Saenger, 1991). Their prevalence and strategic location reflect hydrogen-bonding versatility, and their intermediate strength allows for a great sensitivity to environmental factors (water, ions, etc.). To further our understanding of the structural principles underlying the stability of biological systems, theoretical as well as experimental techniques that can differentiate among a variety of environmental hydrogen-bonding contexts are needed. Among theoretical methods, molecular dynamics (MD) simulations allow, in principle, for the analysis of all components of the model system for both dynamic and time-averaged properties and are therefore an ideal tool for testing and expanding our present understanding of the dynamics of the interactions involved in the stabilization of nucleic acid structures, especially DNA (McCammon and Harvey, 1987; Westhof and Beveridge, 1990; Beveridge and Ravishanker, 1994; Louise-May et al., 1996). However, MD simulations on RNA systems reveal stability and equilibrium problems more severe than in case of DNA (Westhof et al., 1995).

In fact, the three-dimensional structure of ribonucleic acids, and more specifically of tRNA (for a review see Dirheimer et al., 1995), exemplifies several specialized contexts for hydrogen-bonding interactions not present in DNA systems and highlights their role in recognition processes as well as in the stabilization of specific conformations. This is especially true for nonhelical regions where both a high occurrence of modified residues and unusual internucleotide interactions are present. The tRNA^{Asp} anticodon hairpin (Fig. 1) regroups some of these features. It contains a pseudo-uridine (Ψ32) and a N1-methylated guanine (m^{1}G37) in the loop region as well as a G · · · U "wobble" base pair (G30 · · · U40) in the stem. The folding of the anticodon hairpin results from a U-turn motif (Quigley and Rich, 1976) identified also in the tRNA^{Asp} thymine loop (Westhof et al., 1985) and in the two recent hammerhead ribozyme crystal structures (Pley et al., 1994; Scott et al., 1995).

Although nucleic acid tertiary interactions have been described mainly in terms of classical hydrogen bonding between polar atoms, other types of interaction that are less well understood, such as C—H · · · O hydrogen bonds, may play a role in the stabilization of complex RNA folding patterns. For nucleic acids, it was suggested that C—H · · · O interactions contribute to the stabilization of standard base pairs and mismatches (Leonard et al., 1995), and a RNA hexamer crystal structure containing a *trans* U–U base pair stabilized by a classical C4–O4 · · · H3–N3 and a nonclassical C5–H5 · · · O4 hydrogen bond was recently described (Wahl et al., 1996). The reality of C—H · · · O contacts is further supported by neutron diffraction data of small crystal hydrates (Taylor and Kennard, 1982; Steiner and Saenger, 1992) and analysis of protein x-ray structures

Received for publication 6 March 1996 and in final form 29 April 1996.
Supplemental material will be found on the Biophysics Internet server. For instructions, see the Biophysics on the Internet page at the end of this issue.
Address reprint requests to Dr. Eric Westhof, Institut de Biologie Moléculaire et Cellulaire, 15 rue René Descartes, 67084 Strasbourg Cedex, France. Tel.: 33-88-41-70-46; Fax: 33-88-60-22-18; E-mail: Westhof@ibmc. u-strasbg.fr.

0006-3495/96/08/940/15 $2.00

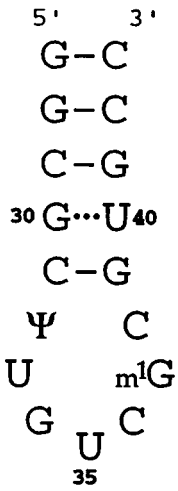

FIGURE 1 Secondary structure representation of the $tRNA^{Asp}$ anticodon loop. Ψ and m¹G notations refer to the nonstandard pseudo-uridine and 1-methylguanine residues.

(Derewenda et al., 1995). C—H groups were also found to establish hydrogen bonds with water oxygen atoms (Steiner and Saenger, 1993). From a previous MD study of the $tRNA^{Asp}$ anticodon hairpin (Auffinger et al., 1996b), several nonstandard C—H · · · O interactions have been dynamically characterized and, for a model of a solvated $tRNA^{Asp}$ molecule, the importance of potential C—H · · · O w contacts has been discussed (Auffinger et al., 1996a).

Unfortunately, the dynamical characterization of canonical and noncanonical base-pairing schemes, such as those described above, still remain beyond the resolution of experimental techniques. At the same time, methodological drawbacks of the MD method associated with approximations introduced by time-saving techniques such as truncation of long-range electrostatic interactions result in unacceptable divergences from experimental data and, for biomolecular systems, disruption of important tertiary interactions on short time scales (Smith and Pettitt, 1991; Schreiber and Steinhauser, 1992a,b,c; Auffinger and Beveridge, 1995; Cheatham et al., 1995; Auffinger et al., 1996b). In nucleic acid MD simulations, base-pair opening events were observed on the 100-ps time scale (Miaskiewicz et al., 1993), whereas a millisecond time scale for such processes is indicated by NMR experiments (Kochoyan et al., 1990; Moe and Russu, 1990). This strongly suggests that the main tertiary interactions present in the starting structure, usually a crystallographic reference, should be maintained on the nanosecond time scale accessible to current MD simulations. The Ewald summation methods used for the calculation of electrostatic interactions avoid the issue of truncation of long-ranged forces by constructing and exploiting system periodicity (Allen and Tildesley, 1987). Recent simulations of DNA oligonucleotides (Cheatham et al., 1995; Lee et al., 1995b; York et al., 1995), triple helices (Weerasinghe et al., 1995a,b) and RNA systems (Cheatham et al., 1995; Lee et al., 1995a; Zichi, 1995) using Ewald or particle mesh Ewald (PME) methods have demonstrated their ability to generate stable MD trajectories extending into the nanosecond time scale. This advance permits consideration of numerous biochemical questions previously beyond the resolution of macromolecular theoretical models.

Among them, the issue of conformational space sampling, which needs simulations on long time scales, is of particular importance. Yet, extension of the MD time scale does not warrant a more accurate representation of the conformational states accessible to a given system. Slow accumulation of errors at each time step owing to slight inaccuracies in the force field or in the simulation protocol may need several hundreds of picoseconds to be detected and may induce a drift of the calculated trajectory from the real conformational space, the slope of this drift being proportional to the accuracy of the simulation protocol. Therefore, a clear evaluation of the reliability and consistency of the structural results is essential. The multiple molecular dynamics (MMD) strategy, which consists in generating several MD trajectories starting from the same point of the conformational space by slightly modifying the simulation protocol, exploits the initial condition sensitivity of MD methodology as a tool for testing the stability of the MD protocol while addressing at the same time the issue of conformational sampling (Auffinger et al., 1995, 1996b; Louise-May et al., 1995). An assessment of the convergence of an MMD trajectory set helps in evaluating the extent of protocol stability and gives an indication of the reliability of the results extracted from a given set of MD trajectories. Further, the comparative analysis of the generated trajectories permits an evaluation of the stability of the tertiary interactions present in the system under study.

We report on an MMD set of six 500-ps MD trajectories (S1–S6), totaling 3 ns of simulations on the 17-base-long $tRNA^{Asp}$ anticodon hairpin (Fig. 1). One of the main goals of the study was to assess the level of structural stability achieved through the use of the PME method for the treatment of long-range electrostatic forces by examining the dynamical behavior of the main tertiary interactions, which should be maintained on the present time scale. A test of the accuracy of the simulations will be given by the description of the dynamical behavior of the two C—H· · · O bonds identified in the tRNA anticodon loop. The solvation features of the system will be presented in a forthcoming communication (Auffinger and Westhof, unpublished results).

COMPUTATIONAL PROCEDURES

The AMBER4.1 software package (Pearlman et al., 1994) was used to run a series of six 500-ps simulations of the 17-base-long $tRNA^{Asp}$ anticodon hairpin (Fig. 1). The hairpin was neutralised by 16 NH_4^+ counterions and solvated by 1143 SPC/E water molecules (Berendsen et al., 1987), filling a 47.3 Å × 33.7 Å × 32.7 Å rectilinear box. We ran

the trajectories at constant temperature (298 K) and constant pressure (1 atm), using a 2-fs time step. The nonbonded pair list was updated every 10 steps. The starting coordinates were kept the same for each simulation by use of the solute coordinates from the $tRNA^{Asp}$ crystal structure (NDB code tRNA05; Westhof et al., 1985) extracted from the nucleic acid database (Berman et al., 1992). To avoid problems associated with the truncation of long-ranged electrostatic forces, the PME method (Darden et al., 1993; York et al., 1993; Essmann et al., 1995), implemented in the AMBER 4.1 package, was employed. A 9.0-Å truncation distance was applied to the Lennard–Jones interactions. The charge grid spacing was chosen close to 1.0 Å, and a charge grid cubic interpolation scheme was used. These parameters were previously shown to effect a good compromise between calculation accuracy and CPU time consumption (York et al., 1993). As in our earlier studies of this system (Auffinger et al., 1995, 1996a,b; Louise-May et al., 1995), we employed the Pearlman–Kim set of electrostatic point charges derived from low-temperature x-ray data of isolated nucleotides (Pearlman and Kim, 1990). The charges for the modified residues Ψ32 and m^1G37 were adapted from those of the standard bases. NH_4^+ counterions were used to neutralize the system, with NH_4^+ parameters developed by Singh et al. (1987).

The equilibration protocol is similar to those used in our preceding research on tRNA and tRNA fragments (Auffinger et al., 1995, 1996b; Louise-May et al., 1995) and consisted of 100 steps of steepest descent minimization applied to the solvent molecules with fixed solute. Then 5 ps of molecular dynamics ensued at 300 K on the water molecules with fixed RNA and NH_4^+ counterion positions. Next followed MD of mobile counterions and water molecules at temperatures of 100 K (1 ps), 200 K (1 ps), and 300 K (5 ps) with fixed RNA positions. In subsequent steps, no position constraints were applied to the system. The temperature was progressively increased to 298 K in steps of 50 K with 1 ps of MD at each step. Finally, at 298 K, 5 ps of dynamics were run to allow the system to equilibrate at room temperature. The thermalization and equilibration phase of the MD protocol thus lasted 22 ps. For each simulation, data were collected over the subsequent 500 ps of trajectory. At each temperature increase the velocities were reassigned randomly according to a Boltzmann distribution. To generate decorrelated trajectories starting from exactly the same initial configuration, different values of the random seed for the velocity distribution assignment were used at the 50-K restart (Auffinger et al., 1995). The SHAKE algorithm was employed at all stages of the simulation to constrain each X—H bond of the system. A 10-kcal mol^{-1} $Å^{-2}$ harmonic distance constraint was applied to the three hydrogen bonds of the first GC base pair to prevent stem from fraying. We used the MD Draw program (Engler and Wipff, 1994) to visualize the generated trajectories on a Silicon Graphics workstation.

RESULTS AND DISCUSSION

In the following sections a comparison of the dynamical features of the six uncorrelated MD simulations (S1–S6) is made. First, the level of convergence achieved for these trajectories on the 500-ps time scale is estimated by analysis of time-dependent root-mean-square (rms) deviations from the crystallographic structure. Then a detailed evaluation of the stability of the main tertiary interactions that structure the anticodon hairpin, including analyses of dihedral angle transitions and a comparison of crystallographic and MD calculated Debye–Waller or *B* factors, is presented.

Global rms deviations

Fig. 2 displays the time-dependent rms deviations from the crystal structure for all six trajectories. The rms deviations for the average trajectory, obtained by calculating the average structure at each time step, are plotted as a heavy black curve. For clarity, we smoothed the curves by using a weighting function. The unmodified curves are plotted in the inset. In Fig. 3 we display a superposition of the last 100-ps average structure of each trajectory on the starting crystallographic reference structure.

From Fig. 2, the diversity of the individual trajectory profiles is apparent and results in final 100-ps all-atom average rms deviation values in the 1.4–2.5-Å range (Table 1; these values were calculated over the last 100 ps of the entire 500-ps trajectories so that we would not overrepresent conformations close to the starting crystallographic reference). The absence of unidirectional drift to higher values of

TABLE 1 Cross RMS deviations calculated between the average structures computed over the last 100 ps of each trajectory, including the average trajectory and the x-ray structure.

	X Ray	S1	S2	S3	S4	S5	S6	S Avg
X Ray	/	1.4	2.2	2.5	2.1	1.4	2.0	1.7
S1		/	1.6	2.0	1.6	1.4	1.5	1.1
S2			/	1.7	1.2	1.9	1.2	0.9
S3				/	1.2	**2.7**	1.4	1.3
S4					/	2.2	**0.5**	0.7
S5						/	2.0	1.7
S6							/	0.7
S Avg								/

The highest and lowest calculated rms deviations are in boldface type.

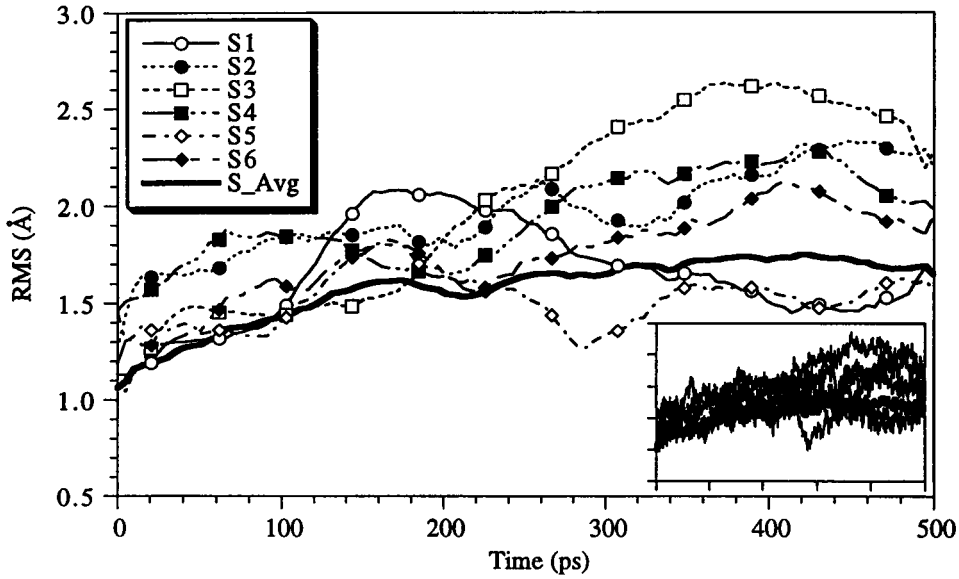

FIGURE 2 Superposition of the curves representing the all-atom total rms deviations with respect to the crystal structure. For clarity, the main curves have been smoothed; the curves in the inset are unmodified. In both the figure and the inset the curves corresponding to the average trajectory have been plotted as heavy black curves.

the rms deviations reveals a good level of structural stabilization according to current MD standards. The final value for the average trajectory rms deviations, reflecting an average over time and different conformational paths, is close to 1.7 Å. This rms value can be compared with the final values close to 1.5 Å obtained for a 200-ps trajectory of a 12-base-long RNA tetranucleotide hairpin by the classical Ewald summation method (Zichi, 1995) and for a single 1-ns MD trajectory of a different 12-base-long RNA tetranucleotide hairpin sequence by the PME method (Cheatham et al., 1995). The slightly higher rms deviations calculated for the 17-nucleotide anticodon hairpin might be reflecting the experimental increase in thermal stability of four instead of seven nucleotide loops.

FIGURE 3 Stero view of the superposition of the final structures, averaged over the last 100 ps of each of the six trajectories, with the crystal structure displayed as bold curves.

Comparisons of the range of global rms deviations of the present MMD trajectories with that of our two previous MMD studies, which employed 8-Å (Auffinger et al., 1995) and 16-Å (Auffinger et al., 1996b) solvent interaction truncation distances, revealed a significant increase in structural stability of the present trajectories generated with the PME method. The use of 8- and 16-Å solvent truncation methods resulted in 1.8–3.9- and 1.6–3.0-Å ranges, respectively, of final rms deviations after 100 ps, whereas for the present set the calculated rms deviations after 100 ps are in the 1.4–1.8-Å range. Reduction of the global rms deviations from use of the PME method over a short 9-Å solvent interaction truncation scheme was also recently reported (Cheatham et al., 1995). This decrease in rms deviations emphasizes the effect of long-range solvent forces in biomolecular tertiary structure stabilization (Auffinger et al., 1996b), as in both comparative studies all solute–solute interactions were calculated explicitly. Further, these results, along with other studies of proteins (Kitson et al., 1993; York et al., 1993; Saito, 1994; York et al., 1994), nucleic acids (Cheatham et al., 1995; Lee et al., 1995b; York et al., 1995), smaller molecular systems (Smith and Pettitt, 1991; Schreiber and Steinhauser, 1992a,b,c) and ionic solutions (Auffinger and Beveridge, 1995; Perera et al., 1995) emphasize the need for calculation of all long-range interactions with the highest possible precision to avoid artifacts associated with the use of truncation schemes.

Experimental and calculated per-residue *B* factors

To compare directly our MD results with experimental data, we calculated, over the last 100 ps of each trajectory, the profiles of the per-residue *B* factors (Fig. 4). *B* factors were calculated from the atomic fluctuations $\langle \delta r^2 \rangle^{1/2}$ by the for-

mula $B = (8\pi^{2/3})\langle \delta r^2 \rangle$ and compared with the experimental B factors obtained for the full $tRNA^{Asp}$ crystal structure (Westhof et al., 1985) represented by the thin solid curve in Fig. 4. Although the comparison reveals larger fluctuations in solution than in the crystal as calculated from our simulations, the order of magnitude of the mobilities is comparable. The lower mobilities of the end residues in the crystallographic reference can be attributed, in part, to the connection of the anticodon fragment to the rest of the tRNA structure. Additionally, crystallographic base-paired contacts among the G34, U35, and C36 anticodon residues of symmetrically related tRNA molecules, mimicking codon–anticodon interactions (Moras et al., 1986), can also reduce the mobility of the loop. In fact, the nearly uniform crystallographic B factors for the loop residues U33 to m^1G37 in the anticodon region (close to 30 $Å^2$) hint at the possibility that crystal packing forces could be masking local dynamical heterogeneity revealed in the MD calculated values, i.e., the high MD calculated mobility of the G34 apical residue at the "wobble" position. The special mobility of this residue certainly plays a role in the wobbling pairing rules necessary for proper biological function of the anticodon.

Cross-rms deviations

Although a good level of consistency for this set of trajectories is demonstrated by the per-residue B-factor profiles, the range of global time-dependent rms deviations (Fig. 2) and the superposition of the final average structures (Fig. 3) reveal a sufficient variety of dynamical features to raise the question of the structural convergence achieved by this set of MMD simulations. Calculated cross-rms deviations between the average structures taken over the last 100 ps of each trajectory are used here to give an initial gross estimate of the differences among the six trajectories (Table 1). The cross-rms values range from 2.7 Å between S3 and S5 to a 0.5-Å rms deviation between S4 and S6. Consequently, S3 and S5 appear to have divergent dynamical behavior and explore significantly different regions of the phase space, whereas S4 and S6 may move along distinct paths in the same region of the phase space. As a set, the six trajectories could be argued to be sampling at least five different regions of phase space on the 500-ps MD time scale.

In the next sections, precise delineation of the differences and similarities among these trajectories will be made based on analyses of backbone dihedral angle transitions and on the stability of classical and nonclassical tertiary hydrogen bonds in stem and loop regions.

Backbone dihedral angle transitions

The number of backbone dihedral angle transitions is a good indicator of the structural stability of MD trajectories. In our simulations, no transitions are observed for the O5′–C5′ and C4′–C3′ angles, and a very small number of transitions are found for the C3′–O3′ and O3′–P angles, respectively 0.1 and 0.2 transitions per 100 ps over the 3 ns of the six trajectories (Table 2). The most frequent transitions are observed in the C5′–C4′ and P–O5′ angles, respectively 1.0 and 1.6 transitions/100 ps. The total number of transitions/100 ps averaged over all types of backbone dihedral angles and over the entire 3 ns of simulation is 2.9. This number can be compared with the numbers of dihedral angle transitions/100 ps calculated in our earlier studies of the same system: 6.5 and 15 transitions/100 ps, using respectively, 8- and 16-Å solvent truncation distances (Auffinger et al., 1996b). This effect demonstrates once more the stabilizing effect of the long-range solvent interactions. A large percentage of the total number of transitions, 62 of 88, are reversible on the 500-ps time scale with lifetimes in the 5–200-ps range. The reversibility of the remaining 26 transitions cannot be excluded on longer time scales. This result points to the necessity of performing MD simulations over time scales at least 1 order of magnitude longer than the transitions that display the highest relaxation times (van

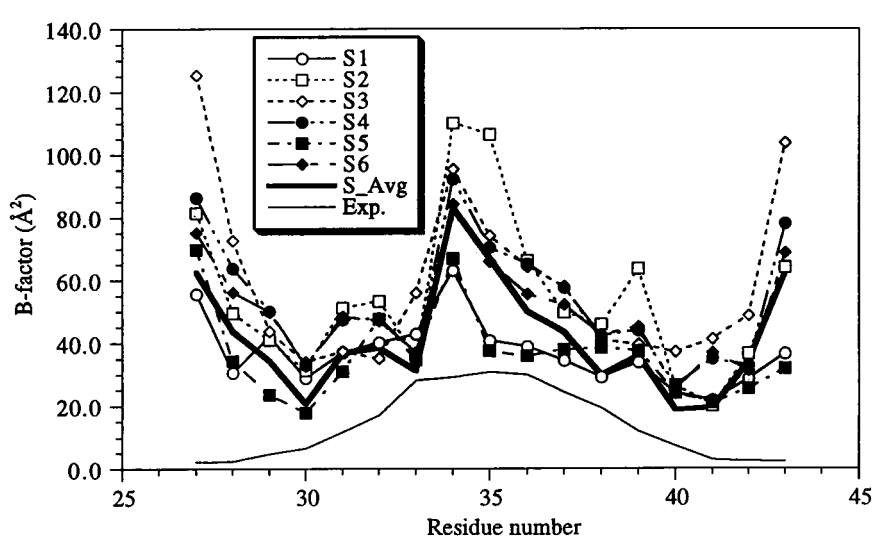

FIGURE 4 Superposition of the curves representing the per-residue B factors calculated over the last 100 ps of each trajectory. The heavy black curve corresponds to the average trajectory, and the thin solid curve corresponds to the experimental B factors.

TABLE 2 Average number of backbone dihedral angle transitions/100 ps of simulation calculated for the six 500-ps trajectories

Transitions	S1	S2	S3	S4	S5	S6	Average
P-O5′–C5′–C4′	None	None	None	None	None	None	None
O5′–C5′–C4′–C3′	1.0	0.8	1.2	0.8	0.8	1.6	1.0
C5′–C4′–C3′–O3′	None	None	None	None	None	None	None
C4′–C3′–O3′–P	None	0.2	0.4	0.2	None	0.2	0.2
C3′–O3′–P–O5′	None	None	0.4	None	None	0.2	0.1
O3′–P–O5′–C5′	0.6	1.2	1.0	2.8	0.8	3.4	1.6
Total	1.6	2.2	3.0	3.8	1.6	5.4	2.9

Dihedral transitions are defined as transitions between minima centered, respectively, on the g^+ (+60°), the g^- (−60°), and the t (180°) domains.

Gunsteren, 1990; van Gunsteren and Mark, 1992) to get an accurate idea of the dihedral angles' conformational behavior. The careful characterization of the dihedral angle dynamical behavior is needed to provide useful comparison points between NMR experiments and MD trajectories, as dihedral angle constraints have been shown to improve the precision of RNA backbone conformation determinations and are increasingly being included in NMR refinements (Cheong et al., 1990; Allain and Varani, 1995; Moore, 1995).

Table 3 lists the number and location of dihedral angle transitions for each of the six MD trajectories. However, a general correlation between number, location, or both of dihedral angle transitions and global rms deviation behavior is not apparent. For example, although simulation S3 displays a high 2.5-Å final rms deviation, it shows no dihedral transitions in the loop region and only a small number in the stem region, mostly for the G27 end residue backbone. More generally, instead of trying to characterize the different behaviors of specific residues, we found that residues G28, Ψ32, m^1G37, C38, and G39 have phosphodiester torsion angles that are not subject to transitions, wherease residues U33, U35, and U40 reside in more conformationally flexible regions of the anticodon fragment. It can also be noted that the backbones of C29 and G34 display a substantial number of nonreversible transitions on the present time scale. Looking down the sequence and comparing across the six trajectories, we found a fair amount of dynamical heterogeneity in the dihedral angle dynamical characteristics of both stem and loop regions.

Among all these transitions, 14 "crankshaft motions" (Olson, 1981; McCammon and Harvey, 1987, p. 112), defined as correlated transitions of the backbone torsion angle P–O5′ and the succeeding C5′–C4′, are identified. These "crankshaft motions" occur in the stem region at the C29–G30, G30–C31, and G41–C42 internucleotide linkages as well as in the loop region between residues G34–U35 and U35–C36. Four of these transitions are reversible on the present time scale. In all cases, first the P–O5′ transition takes place, followed, either immediately or within 30 ps, by the C5′–C4′ transition. For the reverse transitions, the inverse order occurs: first the C5′–C4′ transition, followed by

TABLE 3 Total number of backbone dihedral angle transitions observed over the 500 ps of each trajectory for each nucleotide of the anticodon hairpin

Residue	S1	S2	S3	S4	S5	S6	Total
Stem							
G27	3 (2)	2 (2)	11 (10)	–	2 (2)	–	18 (16)
G28	–	–	–	–	–	–	–
C29	–	1	–	1	–	1	3
G30	2 (2)	1	–	1	–	1	5 (2)
C31	2 (2)	–	–	–	–	–	2 (2)
Loop							
Ψ32	–	–	–	–	–	–	–
U33	1	2 (2)	–	2 (2)	–	7 (6)	12 (10)
G34	–	2	–	2	1	3	8
U35	–	1	–	3 (2)	1	7 (6)	12 (8)
C36	–	2 (2)	–	–	–	6 (6)	8 (8)
m^1G37	–	–	–	–	–	–	–
C38	–	–	–	–	–	–	–
Stem							
G39	–	–	–	–	–	–	–
U40	–	–	2 (2)	8 (8)	3 (2)	2 (2)	15 (14)
G41	–	–	1	2 (2)	1	–	4 (2)
C42	–	–	1	–	–	–	1
C43	–	–	–	–	–	–	–

The number of reversible transitions is given in parentheses. Dihedral transitions are defined as transitions between minima centered, respectively, on the g^+ (+60°), the g^- (−60°), and the t (180°) domains.

the O5′–P transition. Zichi (1995) likewise noted the occurrence of such transitions in a 200-ps-long simulation of a tetranucleotide RNA hairpin. "Crankshaft motions" have been described as well in simulations of B-DNA oligonucleotides (Singh et al., 1985; Swaminathan et al., 1991; Beveridge and Ravishanker, 1994; York et al., 1995).

Canonical stem and G · · · U base-pair hydrogen-bond stabilities

Because the hydrogen bonds of the first G27–C43 base pair were constrained to prevent fraying of the stem during the simulation, no breaking events of these hydrogen bonds were observed, and their average calculated values remained close to the crystallographic ones (Table 4). The averaged hydrogen-bond distances for the remaining three G–C base pairs of the stem likewise exhibit values close to the crystallographic ones. The largest hydrogen-bond fluctuations were observed for the external N4–H42 · · · O6 bonds, an effect even more pronounced for the two G–C base pairs flanking the G · · · U stem base pair (Table 4). This is illustrated in Fig. 5, which shows, for simulations S1 and S2, the three time-dependent hydrogen-bond distances for the C29–G41 base pair. For both, the N4–H42 · · · O6 bond displays the highest fluctuations, as noted before. However, whereas the curve corresponding to S1 is relatively stable, short reversible "breaking" events in S2, reflected in the dynamical behavior of the central N3 · · · H1–N1 bond but absent for the distal O2 · · · H21–N2 bond, can be noted. High fluctuations for N4–H42 · · · O6 bonds have also been reported from a 200-ps 12-nucleotide hairpin simulation (Zichi, 1995), and in a 1-ns MD study of a DNA triple helix in saltwater solution a 100-ps-long reversible disruption associated with a water insertion in the N4–H42 · · · O6 bond of a CG–G base triplet was observed (Weerasinghe et al., 1995a).

In the G · · · U "wobble" base pair, significant lability is observed for the "shallow groove" N1–H1 · · · O2 hydrogen bond, whereas the "deep groove" O6 · · · H3–N3 bond remains much more stable during the time course of the simulation, thereby ensuring the structural integrity of this base pair. Again a similar result has been noted by Zichi (1995) for a G · · · U base pair located at the beginning of a 12-nucleotide hairpin stem. In Fig. 6 the hydrogen-bond distances of this base pair are shown for two typical simulations, S3 and S5. In S5 both bonds remain stable for the greatest part of the trajectory; in S3 a rapid hydrogen-bond-breaking event occurs after 300 ps, followed by particularly high fluctuations for the N1–H1 · · · O2 hydrogen-bond distance. Graphical examination of the S3 trajectory reveals that this effect cannot be attributed to the unique 50-ps-long (U40)P–O5′ reversible backbone dihedral transition that occurs near 430 ps. Such behavior can be rationalized only by a modification of the complex hydration pattern surrounding this noncanonical base pair.

It is especially interesting to note that no base-pair opening events were observed in the stem region over the 3 ns of

TABLE 4 Average distances and angles involving the hydrogen atoms and the accepting polar atoms of some structurally important hydrogen bonds of the stem and the loop of the anticodon fragment averaged over the last 100 ps of each trajectory

Bonds	Average over trajectories S1–S6*	Exp.‡
Stem hydrogen bonds		
G27-C43§		
O6 · · · H4–N4	1.93 (0.10)	1.92
	147 (14)	161
N1–H1 · · · N3	1.90 (0.07)	1.82
	161 (10)	175
N2–H2 · · · O2	1.90 (0.09)	1.90
	161 (9)	168
G28–C42		
O6 · · · H4–N4	1.90 (0.11)	1.90
	158 (11)	170
N1–H1 · · · N3	1.92 (0.08)	1.82
	164 (8)	176
N2–H2 · · · O2	1.86 (0.09)	1.90
	163 (9)	169
C29–G41		
N4–H4 · · · O6	1.94 (0.18)	1.93
	153 (14)	158
N3 · · · H1–N1	1.93 (0.10)	1.83
	162 (9)	172
O2 · · · H2–N2	1.86 (0.09)	1.89
	161 (9)	175
G30 · · · U40		
O6 · · · H3–N3	1.88 (0.15)	1.83
	156 (11)	168
N1–H1 · · · O2	2.08 (0.36)	1.84
	150 (15)	163
C31–G39		
N4–H4 · · · O6	1.94 (.15)	1.94
	153 (15)	157
N3 · · · H1–N1	1.92 (0.09)	1.83
	160 (10)	169
O2 · · · H2–N2	1.89 (0.10)	1.88
	164 (8)	177
Loop hydrogen bonds		
Ψ32 · · · C38		
O4 · · · H41–N4	2.79 (0.60)	2.89
	98 (13)	105
O4 · · · H42–N4	2.74 (0.63)	2.68
	101 (12)	92
U33 · · · C36		
N3–H3 · · · OA–P	1.72 (0.08)	1.78
	163 (8)	134
O2 · · · H5–C5	2.60 (0.24)	2.16
	147 (17)	166
O2′ · · · H41–N4	4.51 (1.25)	3.5
	137 (13)	140
U33 · · · U35		
O2′ · · · H5–C5	3.16 (0.96)	2.11
	129 (19)	136

*Average distance and angle values are in angstroms and degrees, respectively; rms fluctuations are given in parentheses.
‡Estimated on the basis of crystallographic coordinates of heavy atoms (in angstroms for the distances and degrees for the angles).
§The hydrogen bonds at the first base pair, G37–C43, of the stem are constrained.

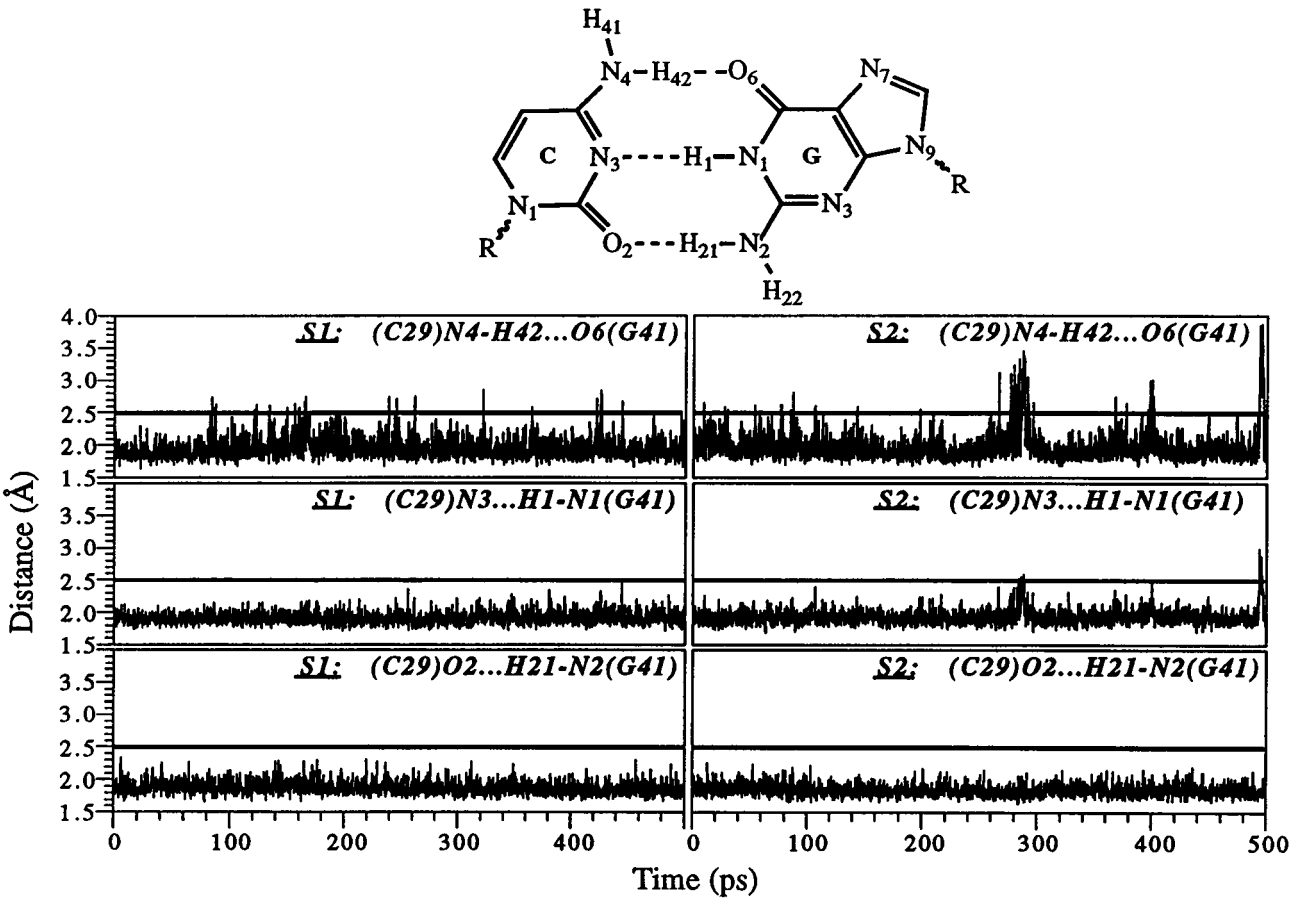

FIGURE 5 Time course of the three G29 · · · C41 base-pair hydrogen-bond distances for simulations S1 and S2. At the top, the Watson–Crick bonds that stabilize this base pair are represented. Curves for all six trajectories are given in the Supplemental Material.

simulations investigated here by the PME method. Such events have been described in numerous MD simulations that used truncation methods for the treatment of the long-range electrostatic interactions. Base-pair opening events have been characterized by NMR experiments on the millisecond time scale (Kochoyan et al., 1990; Moe and Russu, 1990) and thus, on the present time scale, the integrity of the stem base pairs should be well preserved.

In the loop region, tertiary hydrogen-bonding interactions stabilize the three-dimensional structure of the anticodon hairpin. Among these are the C–H · · · O bonds. Their interaction energies have been estimated in the 1–2-kcal/mol range (Desiraju, 1991); they are thus weaker than more classical stem hydrogen bonds. A comparison of the tertiary loop hydrogen-bond stabilities from the 3 ns of MMD trajectories follows.

Ψ32–C38 pseudo-base pair

Ψ32 is the first residue of the seven-base loop and forms a pseudo-base pair with residue C38. These two residues are in close contact in the crystal structure, with an estimated O4 · · · H42–N4 distance and angles of 2.7 Å and 92°, respectively. This interaction, which involves only one hydrogen-bonding contact between the two bases, is maintained even after the formation of the $tRNA^{Asp}$ complex with its cognate synthetase, where the bond distance and angle are 2.1 Å and 103°, respectively (Ruff et al., 1991). Further, in the crystal structure all other loop tertiary interactions are disrupted. From our simulations we observed that this interaction is essentially preserved in trajectories S1, S3, and S5 and that some reversible disrupting events occur in trajectories S2 and S4. The dynamics of this bond is the most dramatic for S6, as can be seen from Fig. 7, where a comparison of the time course of the (Ψ32)O4 · · · N4(C38) distance for simulations S5 and S6 is shown. In Fig. 7 the (Ψ32)O4 · · · N4(C38) distance is used instead of the (Ψ32)O4 · · · H4(1/2)–N4(C38) hydrogen-bonding distances. The latter two hydrogen bonds have very similar average distance and angle values, as indicated in Table 4, which reveals a bifurcated hydrogen-bond geometry. In S6, after approximately 200 ps, the (Ψ32)O4 · · · H4(1/2)-N4(C38) bonds break, re-form between 340 and 400 ps, and break again, but do not re-form on the present time scale, perhaps indicating some irreversible structural transition. The position of Ψ32 in S6 reveals a propensity for that residue to form a pseudo-base pair with m^1G37, without, however, being at any moment within hydrogen-bonding distance. At

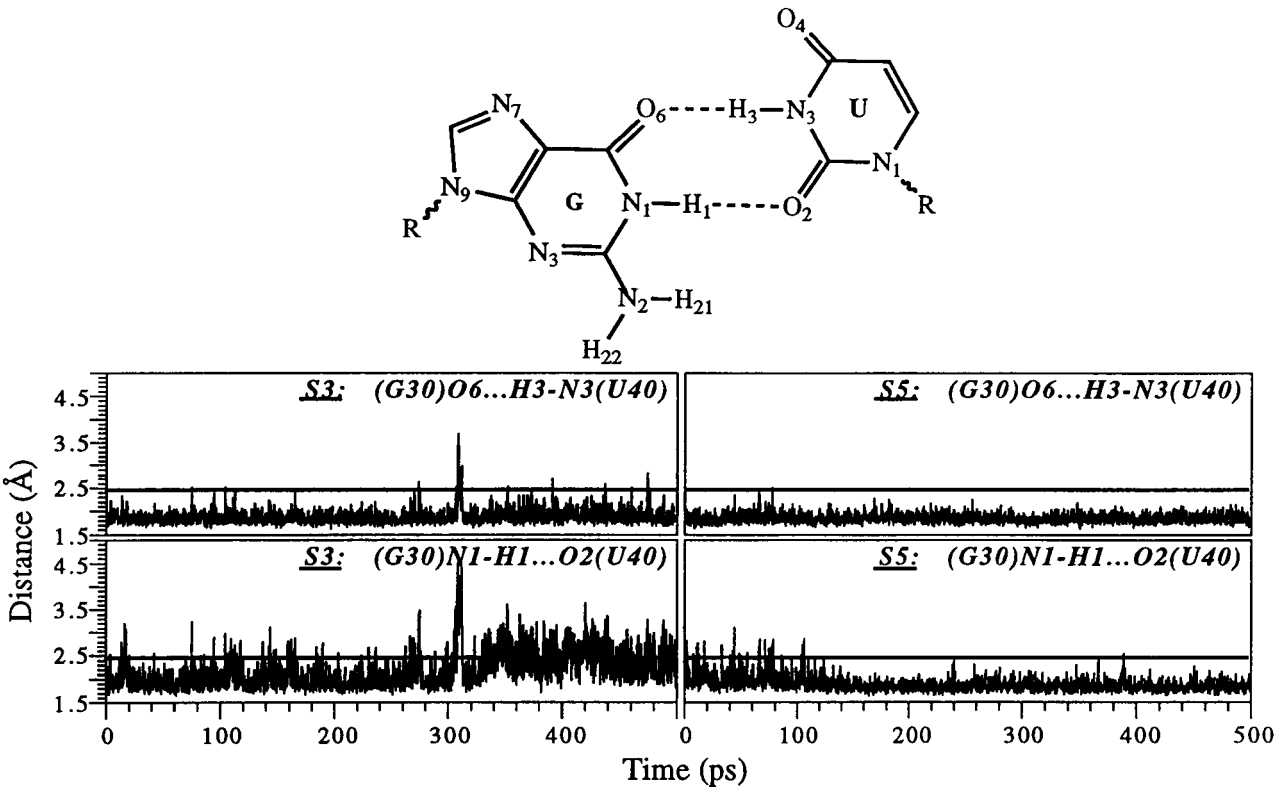

FIGURE 6 Time course of the two G30 · · · C40 "wobble" base-pair hydrogen-bond distances for simulations S3 and S5. At the top, the hydrogen bonds that stabilize this noncanonical base pair are represented. Curves for all six trajectories are given in the Supplemental Material.

the same time, C38 remains in its initial stacked position between m^{1}G37 and G39. Examination of all the existing tRNA crystal structures reveals a situation similar to the one observed in S6 only in the tRNA^{Phe} structure crystallized at pH = 5.0 with Pb^{2+} ions (NDB code tRNA03; Brown et al., 1985). In this structure a lead ion is directly coordinated to the (Y37)N7 site and establishes a 2.9-Å contact with (Cm32)O2, therefore disrupting any water network potentially involved in the stabilization of the Cm32–A38 tRNA^{Phe} pseudo-base pair. In the other tRNA^{Phe} crystal structures an equivalent single bifurcated hydrogen bond is found to help in the preservation of the Cm32–A38 pseudo-base pair (Quigley and Rich, 1976). Further, it has been shown that, for tRNA^{Gly} from *Escherichia coli*, replacing the U in position 32 by a C leads to the loss of the anticodon discriminating ability (Claesson et al., 1995), thus revealing the general importance of this residue and of the 32–38 loop interactions in the tRNA codon reading function.

C–H · · · O interactions involving residue U33

In an earlier set of six shorter 100-ps MMD simulations (Auffinger et al., 1996b), the strong U-turn-specific (U33)N3–H3 · · · OA–P(C36) hydrogen bond was found to be dynamically stable during the entire 600 ps of MMD simulations, wherease the two weaker (U33)O2 · · · H5–C5(C36) and (U33)O2′ · · · H5–C5(U35) C—H · · · O bonds were found to be dynamically stable over only part of the trajectories. In this section we investigate the stability of these loop interactions for the present set of MD simulations on the 500-ps time scale, using the more accurate PME method for the treatment of the electrostatic interactions.

Again, the (U33)N3–H3 · · · OA–P(C36) bond is found to be particularly stable, with an average distance of 1.7 Å and an average angle of 163° (Table 4). The average (U33)O2 · · · H5–C5(C36) hydrogen-bond distances, computed over the last 100 ps of each trajectory, are in the 2.5–2.8-Å range, and the average angles are in the 135–163° range, both in agreement with the ranges for C—H · · · O contacts proposed by Taylor and Kennard (1982), C · · · O distances between 3.0 and 4.0 Å, and C—H · · · O angles between 90 and 180°. In Fig. 8 the (U33)O2 · · · H5–C5(C36) distances for two typical simulations of the set, S2 and S3, are shown. For S2 this bond distance fluctuates between 2.4 and 3.2 Å in an apparent low-frequency mode; for S3 the average distance for this bond at the end of the trajectory fluctuates around 2.5 Å. Inspection of the crystal structure reveals that this part of the hairpin is tightly packed and thus that a large distance between these atoms can result only from a major destabilization of the loop tertiary structure, as observed in simulations conducted with less-accurate MD protocols (Auffinger et al., 1995; 1996b).

The (U33)O2′ · · · H5–C5(U35) interaction displays a wider range of dynamical behavior. It is well maintained

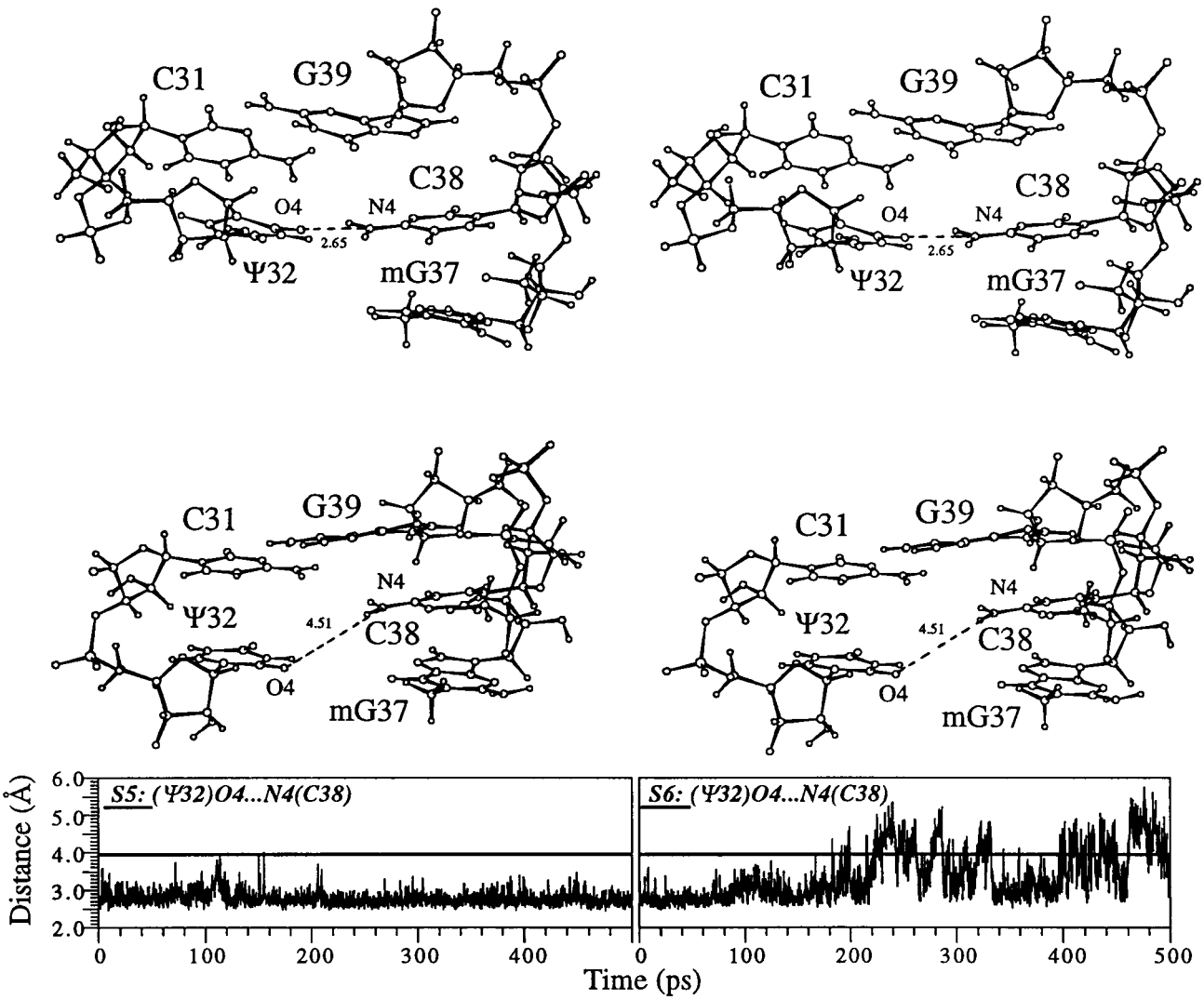

FIGURE 7 At the bottom, the time course of the (Ψ32)O4 · · · N4(C38) distance for simulations S5 and S6 is shown. A snapshot taken from the first 100-ps part of trajectory S6 (*top*) and one from the final 100-ps of the same trajectory (*middle*) are displayed. Curves for all the six trajectories are given in the Supplemental Material.

during simulations S1, S2, S4, and S6, with slightly higher average distances in the 2.7–2.8-Å range and lower angle values, between 101° and 143°. However, for S5 the C—H · · · O distance fluctuations are high, and for simulation S2 an apparently irreversible hydrogen-bond-breaking event, due to water insertion, was recorded (Fig. 8).

To characterize better these C—H · · · O interactions, we present in Fig. 9 two scatterplots of distance versus angles for the (U33)O2 · · · H5–C5(C36) bond. The plots for simulations S1, S3, and S5 are at the right, and those for S2, S4, and S6 are at the left. From these plots it is apparent that two different and almost nonoverlapping hydrogen-bonding distributions are observed. One, shown in the left panel, with rather linear hydrogen bonds, centered on θ(C—H · · · O) ≈ 160° with d(H · · · O) ≈ 2.7 Å, and the other, less linear, centered on θ(C—H · · · O) ≈ 130° with shorter average hydrogen bonding distances: d(H · · · O) ≈ 2.4 Å. A precise analysis reveals that the second type of hydrogen bond is of a rather opportunistic character, occurring as a consequence of conformational changes in the loop that will be described in the following section, whereas the first type is related to unambiguous hydrogen-bonding orientation. However, even in an opportunistic orientation, the short C—H · · · O distances indicate that these interactions contribute somehow to the total stabilization energy.

Thus, with the present simulation protocol and force field, C—H · · · O interactions are maintained over a significant period of time, with average distances and angles in the range of experimentally determined values, i.e., (C—)H · · · O distances less than 3.0 Å and C—H · · · O angles greater than 90°. This result confirms our earlier findings on a shorter 100-ps time scale with a 16-Å solvent interaction truncation distance (Auffinger et al., 1996b) and constitutes a further indication of the possible contribution

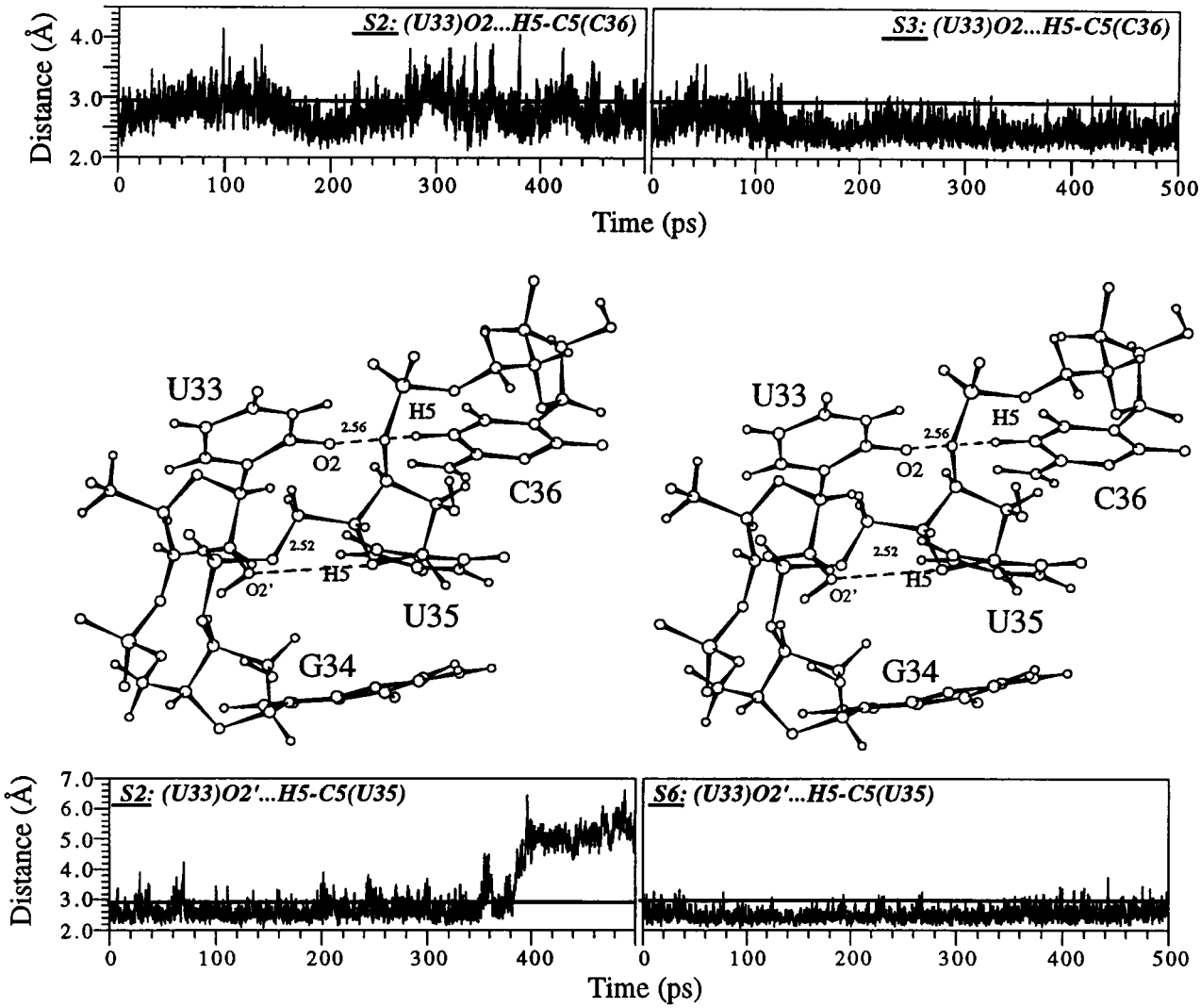

FIGURE 8 Time course of the (U33)O2 · · · H5-C5(C36) hydrogen-bond distance for simulations S2 and S3 (*top*) and for the (U33)O2′) · · · H5–C5(U35) hydrogen-bond distance for simulations S2 and S6 (*bottom*). In the middle, snapshots taken from trajectory S2 are displayed. Curves for all the six trajectories are given in the Supplemental Material.

of such nonclassical hydrogen bonds to the tertiary structural stabilization of nucleic acids, as suggested by other authors on the basis of crystal structure analysis of classical base-paired systems and systems containing mismatches (Leonard et al., 1995; Wahl et al., 1996).

Interactions not present in the crystal structure

MD trajectories allow for structural reorganization, which can give rise to the occurrence of interactions not present in the reference starting structure. The only interaction not present in the crystal structure that we could characterize is the (C36)N4–H41 · · · O2′(U33) hydrogen bond, which formed in only two of the six simulations. In S1 it formed during the equilibration phase, and in S3 it formed after ~100 ps and appears to be particularly stable with average distances and angles near 2.1 Å and 144° (Table 4), respectively. The formation of this bond is accompanied by the creation of a C—H · · · O interaction between atoms (U35)H5 and (U33)O3′ (Fig. 10) but does not involve a disruption of the (U33)O2′ · · · H5–C5(U35) bond. Instead, a bifurcated C—H · · · O bond is formed, leading to a less linear hydrogen-bonding geometry (Fig. 10). Further, this conformational change induces a sliding of the C36 base with respect to the U33 base, leading to less linear C—H · · · O hydrogen bonds, as depicted in the scatterplot in the right-hand panel of Fig. 9. At present, this hydrogen-bonding pattern can be only cautiously proposed as an alternative conformation of the anticodon loop.

Local structural heterogeneity or global conformational changes?

Despite the good level of stability achieved through the use of an improved treatment of long-range electrostatic interactions, these simulations do not converge to a unique set of

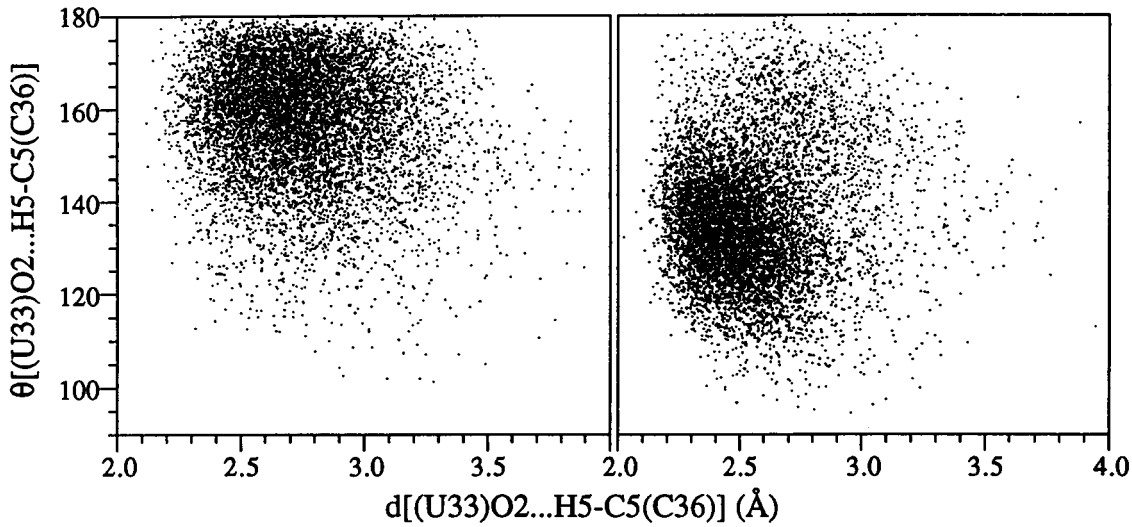

FIGURE 9 Scatter plot of the (C—)H · · · O distances versus C—H · · · O angles for the (U33)O2 · · · H5–C5(C36) hydrogen bond. Values for simulations S1, S3, and S5 are displayed in the left panel, and values for simulations S2, S4, and S6 are displayed in the right panel.

structures but instead reveal a level of structural diversity on the present dynamical time scale. This diversity is reflected by an instability in the (G30)O6 · · · H3–N3(U40) bond for simulation S3; a breaking of the bifurcated pseudo-base-pair bond (Ψ32)O4 · · · H4–N4(C38) for S6; a disruption of the (U33)O2′ · · · H5–C5(U35) bond in S2; the formation of a new (U33)O2′ · · · H41–N4(C36) interaction associated with the bifurcated {(U33)O2′; (U33)O3′} · · · H5-C5(U35) bonds in simulations S1 and S3; and the occurrence of two types of hydrogen-bonding geometry for the (U33)O2 · · · H5-C5(C36) bond (in subsets {S1, S3, and S5} and {S2, S4, and S6}) and associated with the very disparate dihedral angle

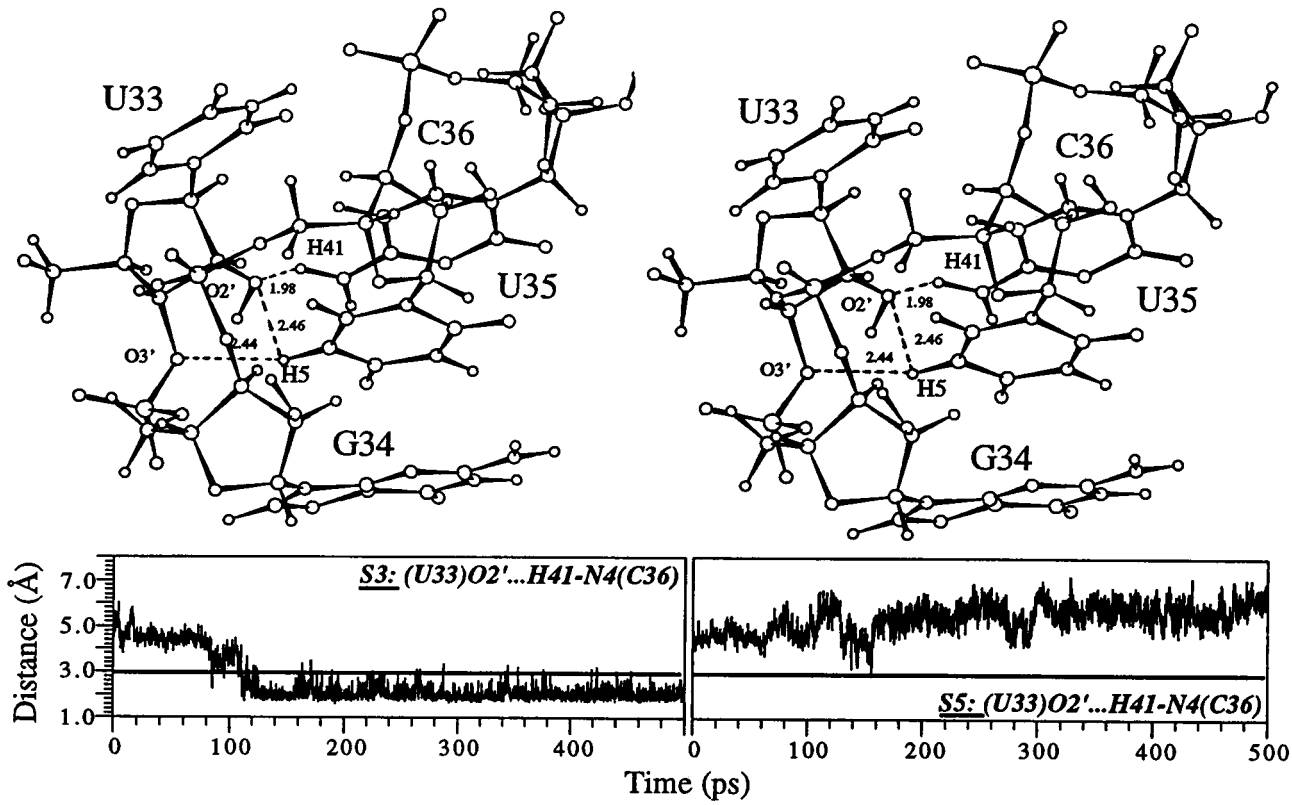

FIGURE 10 Time course of the (U33)O2′ · · · H41–N4(C36) distance for simulations S3 and S5 (*bottom*). At the top, snapshots taken from trajectory S3 are displayed. Curves for all the six trajectories are given in the Supplemental Material.

transitional behavior observed in all these simulations. From these observations no obvious correlation could be inferred between these structural transitions, which would therefore indicate that the structural diversity results more from a local structural than from global conformational changes. It is especially difficult to establish a clear and unambiguous relation between the calculated rms deviations from the crystal structure and the observed transitions. The low 0.5-Å value calculated between the final average structures of S4 and S6 (Table 1) indicated, however, that these two trajectories apparently evolved in closely related regions of the "theoretical" phase space. This is further supported by a similar behavior of the (Ψ32)O4 · · · H4–N4(C38) bond, which shows comparable instabilities in S4 and S6 (see Fig. 3). A general trend inferred from the present set of simulations is that all these trajectories evolve in regions of the "theoretical" phase space close to the initial starting structure but display different local structural transitions. This set of simulations exemplifies, therefore, the great dynamical complexity of this RNA system in solution and allowed us to characterize a dynamical range of potentially accessible states that will serve as a sound basis for further investigations with longer time scales including refined representation of the environment such as the inclusion of structurally important Mg^{2+} ions.

CONCLUSIONS

We have generated six uncorrelated 500-ps MD trajectories of the fully solvated and neutralized $tRNA^{Asp}$ anticodon hairpin, all starting from the same initial configuration and resulting in a total of 3 ns of simulation time. The PME method used to calculate the long-range electrostatic interactions allowed us to generate stable trajectories on the 500-ps time scale with respect to current standards. The calculated rms deviations from the crystal structure remained reasonably low and without the noticeable drifts to higher values that were observed in preceding simulations that used long-range solvent interaction truncation schemes (Auffinger et al., 1996b). These results illustrate the fundamental necessity of an accurate treatment of all long-range electrostatic interactions for reliable modeling studies of highly charged nucleic acids and, more generally, of chemical and biomolecular systems.

Through these improvements and the use of a MMD simulation strategy, a large diversity in the dynamical behavior of the main hydrogen bonds involved in the stabilization of the tertiary structure of this tRNA hairpin was observed and characterized. This diversity is more the result of local structural heterogeneity than of global structural changes. In stems, the G–C base-pair N4–H42 · · · O6 bonds are more labile than the remaining two G–C hydrogen bonds, an effect that becomes even more pronounced for G–C base pairs flanking the "wobble" G · · · U base pair. In G · · · U base pairs the N1–H1 · · · O2 bonds are more labile than the O6 · · · H3-N3 bonds. In the loop the apparently weakly bifurcated (Ψ32)O4 · · · H4–N4(C38) pseudo-base-pair interaction was maintained in at least four of six MD simulations. The two-loop C—H · · · O {(U33)O2 · · · H5–C5(C36) and (U33)O2′ · · · H5-C5(U35)} interactions were found stable during the largest part of these six MD trajectories in either a linear or a bifurcated hydrogen-bonding geometry.

However, the different characteristics displayed by the six trajectories also raise the question of the accuracy limits of present simulations. There is potentially a time-scale limit beyond which such simulations lose their accuracy. The MMD approach used here is useful in gaining such a perspective, because it improves on the statistics of the conformational space that is being sampled, allows for a careful examination of the states accessible to such a system, and questions the reliability of conclusions drawn from structural transitions observed in single MD simulations.

The authors thank Dr. Shirley Louise-May for stimulating discussions and critical comments on the manuscript. P.A. is supported by a fellowship from ORGANIBIO (28, rue Saint Dominique, Paris, France) in the program CM_2AO. The authors are grateful to the IDRIS computing center, which provided computer time, the Peter Kollman AMBER group (UCSF), which provided the latest version of the MD package used for this study, and Georges Wipff and Etienne Engler for the use of their MD Draw display program. E. W. is thankful to the CEE for providing funds through Biotech contract BIO 2-CT93–0345.

REFERENCES

Allain, F. H. T., and G. Varani. 1995. Structure of the P1 helix from group I self-splicing introns. *J. Mol. Biol.* 250:333–353.

Allen, M. P., and D. J. Tildesley. 1987. Computer Simulation of Liquids. Clarendon Press, Oxford.

Auffinger, P., and D. L. Beveridge. 1995. A simple test for evaluating the truncation effects in simulation of systems involving charged groups. *Chem. Phys. Lett.* 234:413–415.

Auffinger, P., S. Louise-May, and E. Westhof. 1995. Multiple molecular dynamics simulations of the anticodon loop of $tRNA^{Asp}$ in aqueous solution with counterions. *J. Am. Chem. Soc.* 117:6720–6726.

Auffinger, P., S. Louise-May, and E. Westhof. 1996a. Hydration of C—H groups in tRNA. *Faraday Discuss.* In press.

Auffinger, P., S. Louise-May, and E. Westhof. 1996b. Molecular dynamics simulations of the anticodon hairpin of $tRNA^{Asp}$: structuring effects of C—H · · · O hydrogen bonds and of long-range hydration forces. *J. Am. Chem. Soc.* 118:1181–1189.

Berendsen, H. J. C., J. R. Grigera, and T. P. Straatsma. 1987. The missing term in effective pair potential. *J. Phys. Chem.* 97:6269–6271.

Berman, H. M., W. K. Olson, D. L. Beveridge, J. Westbrook, A. Gelbin, T. Demeny, S. H. Hsieh, and A. R. Srinivasan. 1992. The nucleic acid database: a comprehensive relational database of three-dimensional structures of nucleic acids. *Biophys. J.* 63:751–759.

Beveridge, D. L., and G. Ravishanker. 1994. Molecular dynamics studies of DNA. *Curr. Opin. Struct. Biol.* 4:246–255.

Brown, R. S., J. C. Dewan, and A. Klug. 1985. Crystallographic and biochemical investigation of the lead-(II) catalyzed hydrolisis of yeast phenylalanine tRNA. *Biochemistry.* 24:4785–4801.

Cheatham, T. E., J. L. Miller, T. Fox, T. A. Darden, and P. A. Kollman. 1995. Molecular dynamics simulations on solvated biomolecular systems: the particle mesh Ewald method leads to stable trajectories of DNA, RNA and proteins. *J. Am. Chem. Soc.* 117:4193–4194.

Cheong, C., G. Varani, and I. Tinoco. 1990. Solution structure of an unusually stable RNA hairpin, 5′GGAC(UUCG)GUCC. *Nature (London).* 346:680–681.

Claesson, C., F. Lustig, T. Borén, C. Simonsson, M. Barciszewska, and U. Lagerkvist. 1995. Glycine codon discrimination and the nucleotide in position 32 of the anticodon loop. *J. Mol. Biol.* 247:191–196.

Darden, T., D. York, and L. Pedersen. 1993. Particle mesh Ewald: an *N* log(*N*) method for Ewald sums in large systems. *J. Chem. Phys.* 98: 10,089–10,092.

Derewenda, Z. S., L. Lee, and U. Derewenda. 1995. The occurrence of C—H · · · O hydrogen bonds in proteins. *J. Mol. Biol.* 252:248–262.

Desiraju, G. R. 1991. The C—H · · · O hydrogen bond in crystals: what is it? *Acc. Chem. Res.* 24:290–296.

Dirheimer, G., G. Keith, P. Dumas, and E. Westhof. 1995. Primary, secondary, and tertiary structures of tRNAs. D. Söll and U. L. Raj Bhandary, editors. *In* tRNA: Structure, Biosynthesis, and Function. American Society for Microbiology, Washington, D.C. 93–126.

Engler, E., and G. Wipff. 1994. MD Draw: a program of graphical representation of molecular dynamics trajectories. Université Louis Pasteur, Strasbourg, France.

Essmann, U., L. Perera, M. L. Berkowitz, T. Darden, H. Lee, and L. G. Pedersen. 1995. A smooth particle mesh Ewald method. *J. Chem. Phys.* 103:8577–8593.

Jeffrey, G. A., and W. Saenger. 1991. Hydrogen Bonding in Biological Structures. Springer-Verlag, Berlin.

Kitson, D. H., F. Avbelj, J. Moult, D. T. Nguyen, J. E. Mertz, D. Hadzi, and A. T. Hagler. 1993. On achieving better than 1 Å accuracy in a simulation of a large protein: *streptomyces griseus* protease A. *Proc. Natl. Acad. Sci. USA.* 90:8920–8924.

Kochoyan, M., J. L. Leroy, and M. Gueron. 1990. Process of base pair opening and proton exchange in Z-DNA. *Biochemistry.* 29:4799–4805.

Lee, H., T. Darden, and L. Pedersen. 1995a. Accurate crystal molecular dynamics simulations using particle-mesh-Ewald: RNA dinucleotides - ApU and GpC. *Chem. Phys. Lett.* 243:229–235.

Lee, H., T. A. Darden, and L. G. Pedersen. 1995b. Molecular dynamics simulation studies of a high resolution Z-DNA crystal. *J. Chem. Phys.* 102:3830–3834.

Leonard, G. A., K. McAuley-Hecht, T. Brown, and W. N. Hunter. 1995. Do C—H · · · O hydrogen bonds contribute to the stability of nucleic acid base pairs. *Acta Cryst.* D51:136–139.

Louise-May, S., P. Auffinger, and E. Westhof. 1996. RNA structure from molecular dynamics simulations. *In* Biological Structure and Dynamics. Proceedings of the Ninth Conversation, Vol. 2. State University of New York. Adenine Press, Albany, NY. 73–90.

Louise-May, S., P. Auffinger, and E. Westhof. 1996. Calculation of nucleic acid conformation. *Curr. Opin. Struct. Biol.* 6:289–298.

McCammon, J. A., and S. C. Harvey. 1987. Dynamics of Proteins and Nucleic Acids. Cambridge University Press, New York.

Miaskiewicz, K., R. Osman, and H. Weinstein. 1993. Molecular dynamics simulation of the hydrated d(CGCGAATTCGCG)2 dodecamer. *J. Am. Chem. Soc.* 115:1526–1537.

Moe, J. G., and I. M. Russu. 1990. Proton exchange and base-pair opening kinetics in 5′-d(CGCGAATTCGCG)-3′ and related dodecamers. *Nucleic Acids Res.* 18:821–827.

Moore, P. B. 1995. Determination of RNA conformation by nuclear magnetic resonance. *Acc. Chem. Res.* 28:241–256.

Moras, D., A. C. Dock, P. Dumas, E. Westhof, P. Romby, J. P. Ebel, and R. Giegé. 1986. Anticodon–anticodon interactions induce conformational changes on tRNA: yeast $tRNA^{Asp}$, a model for tRNA-mRNA recognition. *Proc. Natl. Acad. Sci. USA.* 83:932–936.

Olson, W. K. 1981. Understanding the motions of DNA. *In* Proceedings of the Second SUNYA Conversation in the Discipline Biomolecular Stereodynamics. Adenine, New York. 327–343.

Pearlman, D. A., D. A. Case, J. W. Caldwell, W. S. Ross, T. E. Cheatham III, D. M. Ferguson, G. L. Seibel, U. C. Singh, P. K. Weiner, and P. A. Kollman. 1994. AMBER 4.1, San Francisco, CA.

Pearlman, D. A., and S. H. Kim. 1990. Atomic charges for DNA constituents derived from single-crystal x-ray diffraction data. *J. Mol. Biol.* 211:171–187.

Perera, L., U. Essmann, and M. L. Berkowitz. 1995. Effect of the treatment of long-range forces on the dynamics of ions in aqueous solutions. *J. Chem. Phys.* 102:450–458.

Pley, H. M., K. M. Flaherty, and D. B. McKay. 1994. Three-dimensional structure of a hammerhead ribozyme. *Nature (London).* 372:68–74.

Quigley, G. J., and A. Rich. 1976. Structural domains of transfer RNA molecules. *Science.* 194:796–806.

Ruff, M., S. Krishnaswamy, M. Boeglin, A. Poterszman, A. Mitschler, A. Podjarny, B. Rees, J. C. Thierry, and D. Moras. 1991. Class II aminoacyl tRNA synthetases: crystal structure of yeast aspartyl-tRNA synthetase complexed with $tRNA^{Asp}$. *Science.* 25:1682–1689.

Saito, M. 1994. Molecular dynamics simulations of proteins in solution: artifacts caused by the cutoff approximations. *J. Chem. Phys.* 101: 4055–4061.

Schreiber, H., and O. Steinhauser. 1992a. Cutoff size does strongly influence molecular dynamics results on solvated polypeptides. *Biochemistry.* 31:5856–5860.

Schreiber, H., and O. Steinhauser. 1992b. Molecular dynamics studies of solvated polypeptides: why the cut-off scheme does not work. *Chem. Phys.* 168:75–89.

Schreiber, H., and O. Steinhauser. 1992c. Taming cut-off induced artifacts in molecular dynamics studies of solvated polypeptides. *J. Mol. Biol.* 228:909–923.

Scott, W. G., J. T. Finch, and A. Klug. 1995. The crystal structure of an all-RNA hammerhead ribozyme: a proposed mechanism for RNA catalytic cleavage. *Cell.* 81:991–1002.

Singh, U. C., F. K. Brown, P. A. Bash, and P. A. Kollman. 1987. An approach to the application of free energy perturbation methods using molecular dynamics: application to the transformations of $CH_3OH \rightarrow CH_3CH_3$, $H_3O^+ \rightarrow NH_4^+$, glycine → alanine, and alanine → phenylanaline in aqueous solution and to $H_3O^+(H_2O)_3 \rightarrow NH_4^+(H_2O)_3$ in the gas phase. *J. Am. Chem. Soc.* 109:1607–1614.

Singh, U. C., S. J. Weiner, and P. Kollman. 1985. Molecular dynamics simulations of d(CGCGA) · d(TCGCG) with and without "hydrated" counterions. *Proc. Natl. Acad. Sci. USA.* 82:755–759.

Smith, P. E., and B. M. Pettitt. 1991. Peptides in ionic solutions: a comparison of the Ewald and switching function techniques. *J. Chem. Phys.* 95:8430–8441.

Steiner, T., and W. Saenger. 1992. Geometry of C—H · · · O hydrogen bonds in carbohydrate crystal structures. Analysis of neutron diffraction data. *J. Am. Chem. Soc.* 114:10,146–10,154.

Steiner, T., and W. Saenger. 1993. Role of C—H · · · O hydrogen bonds in the coordination of water molecules. Analysis of neutron diffraction data. *J. Am. Chem. Soc.* 115:4540–4547.

Swaminathan, S., G. Ravishanker, and D. L. Beveridge. 1991. Molecular dynamics of B-DNA including water and counterions: a 140 ps trajectory for d(CGCGAATTCGCG) based on the GROMOS force field. *J. Am. Chem. Soc.* 111:5027–5040.

Taylor, R., and O. Kennard. 1982. Crystallographic evidence for the existence of C—H · · · O, C—H · · · N and C—H · · · Cl hydrogen bonds. *J. Am. Chem. Soc.* 104:5063–5070.

van Gunsteren, W. F. 1990. On testing theoretical models by comparison of calculated with experimental data. *In* Modelling of Molecular Structures and Properties. J. L. Rivaic, editor. Elsevier, Amsterdam. 463–478.

van Gunsteren, W. F., and A. E. Mark. 1992. On the interpretation of biochemical data by molecular dynamics computer simulation. *Eur. J. Biochem.* 204:947–961.

Wahl, M. C., S. T. Rao, and M. Sundaralingam. 1996. Structure of the RNA hexamer, r(UUCGCG), with a 5′-UU-overhang exhibiting Hoogsteen-like trans U · U base pairs. *Nat. Struct. Biol.* 3:24–31.

Weerasinghe, S., P. E. Smith, V. Mohan, Y.-K. Cheng, and B. M. Pettitt. 1995a. Nanosecond dynamics and structure of a model DNA triplex helix in saltwater solution. *J. Am. Chem. Soc.* 117:2147–2158.

Weerasinghe, S., P. E. Smith, and M. Pettitt. 1995b. Structure and stability of a model pyrimidine-purine-purine DNA triple helix with a GC.T mismatch by simulation. *Biochemistry.* 34:16,269–16,278.

Westhof, E., and D. L. Beveridge. 1990. Hydration of nucleic acids. *In* Water Science Reviews 5. F. Franks, editor. Cambridge University Press, Cambridge. 24–123.

Westhof, E., P. Dumas, and D. Moras. 1985. Crystallographic refinement of yeast aspartic acid transfer RNA. *J. Mol. Biol.* 184:119–145.

Westhof, E., C. Rubin-Carrez, and V. Fritsch. 1995. The use of molecular dynamics simulations for modelling nucleic acids. *In* Computer Modelling in Molecular Biology. VCH, New York. 103–131.

York, D. M., T. Darden, and L. G. Pedersen. 1993. The effect of long-range electrostatic interactions in simulations of macromolecular crystals: a comparison of the Ewald and truncated list methods. *J. Chem. Phys.* 99:8345–8348.

York, D. M., A. Wlodawer, L. G. Pedersen, and T. A. Darden. 1994. Atomic-level accuracy in simulations of large protein crystals. *Proc. Natl. Acad. Sci. USA.* 91:8715–8718.

York, D. M., W. Yang, H. Lee, T. Darden, and L. G. Pedersen. 1995. Toward the accurate modeling of DNA: the importance of long-range electrostatics. *J. Am. Chem. Soc.* 117:5001–5002.

Zichi, D. A. 1995. Molecular dynamics of RNA with the OPLS force field. Aqueous simulation of a hairpin containing a tetranucleotide loop. *J. Am. Chem. Soc.* 117:2957–2969.